Chemical Science

EDGE ARTICLE

View Article Online
View Journal | View Issue

Cite this: *Chem. Sci.*, 2018, **9**, 1496

Exploring the mechanism of the Pd-catalyzed spirocyclization reaction: a combined DFT and experimental study†

Ivan Franzoni, ‡[a] Hyung Yoon, ‡[a] José-Antonio García-López, [b] Amalia Isabel Poblador-Bahamonde*[c] and Mark Lautens*[a]

The mechanism of the palladium-catalyzed spirocyclization of acrylamides has been investigated by density functional theory and experimental studies. The results support a mechanistic pathway that proceeds *via* oxidative addition, intramolecular carbopalladation, C–H bond activation, and migratory insertion sequence. The M06L/def2-TZVPP//BP86/6-31G(d,p)/LANL2DZ level of theory used and the inclusion of solvent effects provide results in good agreement with the experimental data. The C–H bond activation step proceeds *via* a concerted *outer*-sphere metallation deprotonation mechanism that explains the absence of a measurable kinetic isotopic effect. The subsequent intermolecular migratory insertion of arynes is significantly faster than the insertion of internal alkynes. Furthermore, the regioselectivities calculated in the case of unsymmetrical reactants are remarkably close to the experimental values. Evaluation of the potential energy surfaces for specific substrates provides an explanation for the lack of product formation observed experimentally. Finally, the computational and experimental analyses of potential side reactions are also presented and support the initially proposed mechanism.

Received 31st October 2017
Accepted 8th December 2017

DOI: 10.1039/c7sc04709f

rsc.li/chemical-science

Introduction

The application of transition metal catalysts in the activation of traditionally inert C–H bonds has advanced significantly and currently represents a recurrent strategy for the construction of carbon–carbon (C–C) and carbon–heteroatom (C–Y) bonds.[1] This approach has opened the possibility to tackle the synthesis of complex molecules based on new disconnections by utilizing simple and inactivated starting materials in a step- and atom-economical fashion.[2] Although substrate prefunctionalization is not required, the installation of a suitable directing group (DG) is necessary in most cases to guide the metal center toward a specific C–H bond in a regioselective manner (Scheme 1a).[3,4] The development of (removable) DGs based on tethered substituted quinolines, pyridines, amides and cyano groups has allowed the intramolecular selective activation and functionalization of C–H bonds in proximal and even distal positions (*e.g. meta*- and *para*-positions in aromatic groups and γ- and δ-positions in alkyl chains).[5,6]

The combination of the palladium-catalyzed intramolecular Mizoroki–Heck reaction and C–H bond activation in a domino process has been exploited as a valuable alternative for the selective functionalization of remote unactivated C–H bonds within the molecular framework (Scheme 1b).[7,8] In this

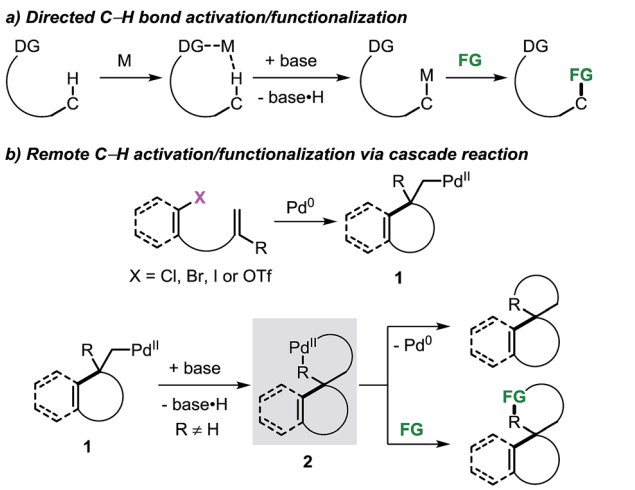

Scheme 1 Remote C–H bond activation and functionalization strategies with the use of directing groups or as a part of a domino process.

[a]*Davenport Research Laboratories, Department of Chemistry, University of Toronto, 80 St. George St., Toronto, Ontario M5S 3H6, Canada. E-mail: mlautens@chem.utoronto.ca*

[b]*Departamento de Química Inorgánica, Universidad de Murcia, Campus de Espinardo, 30100 Murcia, Spain. E-mail: joangalo@um.es*

[c]*Department of Organic Chemistry, University of Geneva, 30 Quai Ernest Ansermet, 1211 Geneva, Switzerland. E-mail: Amalia.pobladorbahamonde@unige.ch*

† Electronic supplementary information (ESI) available: Additional potential energy profiles, additional experimental data, Cartesian coordinates and energies for all intermediates and transition states are given. See DOI: 10.1039/c7sc04709f

‡ These authors contributed equally to this work.

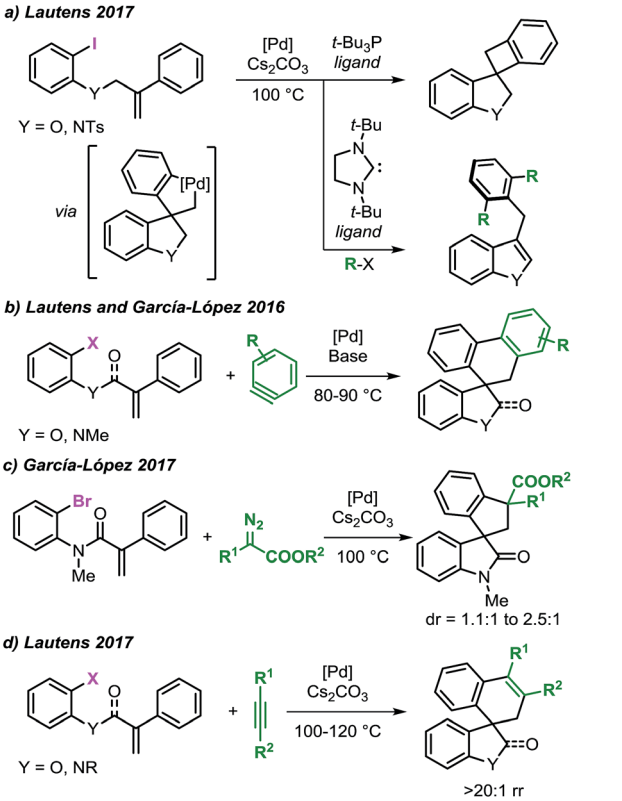

Scheme 2 Synthesis of spiro-heterocycles *via* palladium-catalyzed remote C–H bond activation and functionalization cascade reactions.

approach, a low-valent palladium catalyst undergoes oxidative addition into a carbon–(pseudo)halogen (C–X) bond followed by intramolecular carbopalladation of a tethered unsaturated moiety. This sequence generates σ-alkylpalladium(II) intermediate **1**, where the metal center is now placed in proximity to a formerly remote C–H bond. In the absence of β-hydrogen atoms or nucleophilic species,[9] regioselective C–H bond activation could occur to give the spirocyclic palladacycle **2**. This complex could undergo C–C bond-forming reductive elimination or, in the presence of suitable reactants, further evolve by functionalization of the C–Pd bond.

Inspired by the pioneering work of Grigg[10] and Larock,[11] our groups[12–16] and others[17] have explored this class of transformations for the synthesis of valuable spirocyclic scaffolds containing heterocyclic cores (Scheme 2). These structural motifs have attracted considerable interest due to their occurrence in pharmaceuticals, biologically active, and natural products.[18] In 2014, Shi and co-workers reported the application of this approach in the synthesis of indoline derivatives.[19] Recently, our group disclosed the use of an intramolecular Heck reaction and C–H bond activation cascade for the divergent synthesis of two classes of compounds *via* the intermediacy of a single spirocyclic palladacycle (Scheme 2a).[12] The use of the bulky *t*-Bu_3P ligand promoted the direct C–C bond-forming reductive elimination providing benzofused cyclobutane derivatives. Alternatively, in the presence of alkyl iodides and a N-heterocyclic carbene (NHC) ligand, Catellani-type products were obtained. Following this work, the reactivity of this class of palladacycle intermediates was further explored resulting in the development of several methodologies to access spirooxindoles and spirodihydrobenzofuranes. In 2016, we independently reported the palladium-catalyzed spirocyclization reaction *via* an intramolecular C–H bond activation and aryne migratory insertion sequence (Scheme 2b).[13,14] Extension of this approach to the use of α-diazocompounds[15] and internal alkynes[16] as

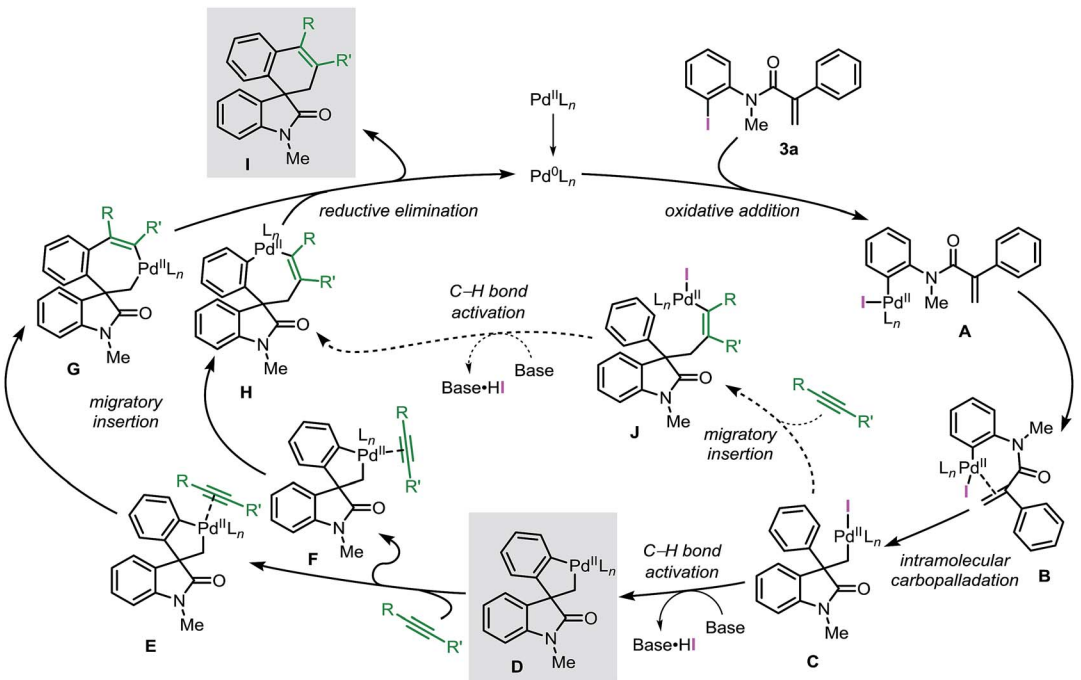

Fig. 1 Initially proposed mechanism for the palladium-catalyzed spirocyclization reaction.

terminating reagents was recently reported by our groups (Scheme 2c and d).

Based on the collective results obtained in these studies, a plausible mechanism for the Pd-catalyzed spirocyclization reaction of unsaturated reagents is presented in Fig. 1.

Initially, the low-valent active catalyst oxidatively adds to the starting material **3a** to form intermediate **A**. Coordination of the tethered double bond functionality to the metal center gives **B** followed by an intramolecular carbopalladation to generate neopentyl intermediate **C**. The lack of β-hydrogen atoms and the conformational flexibility of **C** allow the metal center to be placed in proximity of an *ortho* C(sp^2)–H bond of the phenyl ring. This orientation facilitates a base mediated C–H bond activation process and formation of the spirocyclic palladacycle intermediate **D**. Ligand exchange at the metal center provides either intermediate **E** or **F** where the unsaturated substrate (aryne or alkyne) coordinates to the palladium atom *trans* with respect to either the C(sp^3)–Pd or the C(sp^2)–Pd bond, respectively. Subsequent migratory insertion generates intermediates **G** or **H**, which finally undergo C–C bond-forming reductive elimination, releasing product **I** and the active catalyst. In an alternative scenario, migratory insertion of the unsaturated reactant in **C** precedes the C(sp^2)–H bond activation step to eventually generate complex **H** *via* intermediate **J**.

Recently, the García-López group reported a detailed study on the organometallic intermediates involved in this reaction.[20] Several key species were synthesized and fully characterized by nuclear magnetic resonance and single-crystal X-ray crystallography. Furthermore, the reactivities of these species were evaluated and the role of ligands and bases were studied providing additional insights into the reaction mechanism.

Herein, we report a complementary computational and experimental study on the mechanism of the palladium-catalyzed spirocyclization reaction. Our results support the initially proposed mechanism (Fig. 1) and provide new insights into key steps of the catalytic cycle. Two possible pathways for the C–H bond activation step were computed and the equilibration of several species was studied. Analysis of the migratory insertion step for diverse unsaturated reactants was evaluated and correlated with experimental data. The theoretical results obtained in this study, as well as experimental findings were compared to obtain a comprehensive and realistic overview of the underlying mechanism of these reactions. We anticipate that these results will aid the design of new catalysts, new substrates and novel approaches to extend the applicability of the palladium-catalyzed spirocyclization reactions in the synthesis of other important classes of spirocyclic compounds.

Computational details

The computational studies were performed using acrylamide **3a** as a substrate. This compound was demonstrated to be reactive under both sets of reaction conditions (benzyne and alkyne insertion reactions) and it was successfully employed in the synthesis and isolation of the fully characterized palladacycle complex **11**. All geometries were fully optimized in gas phase at the BP86 level[21] of theory without any constraints, at 298 K and 1 atm using a fine integration grid. The Berny algorithm was used for geometry optimizations.[22] The standard double-ζ basis set (LANL2DZ)[23] and effective core potentials (ECPs)[23c,d] were used for Pd, Cs and heavy halogen atoms whereas for the other atoms (C, H, O, N, P and F) the 6-31G(d,p) Pople basis set was used.[24] Frequency calculations were performed at the same level for all intermediates and transition states to confirm minima (no imaginary frequencies) and first order saddle points (one imaginary frequency representing the desired reaction coordinate), respectively. Furthermore, transition states were confirmed by either intrinsic reaction coordinates (IRC)[25] or quick reaction coordinate (QRC) calculations.[26] The latter calculations were performed by small manual displacement (0.05–0.10 Bohr) of the geometry on the vibration of the imaginary frequency followed by regular optimization. Single point energies were calculated on the optimized structures at 298 K and 1 atm at the M06L level of theory,[27] a method in which dispersion effects are included in the parameterization scheme. The Karlsruhe triple-ζ Gaussian basis set def2-TZVPP was used for all atoms.[28] Solvent effects were assessed through the integral equation formalism variant of the polarizable continuum model (IEFPCM)[29] with default parameters for toluene and UFF radii. Evaluation of other functionals, basis sets, implicit models to describe solvent effects, and with or without addition of the Grimme's D3 dispersion[30] provided qualitative consistent results. Solution phase zero-point corrected energies, enthalpies and Gibbs free energies were obtained by adding the respective gas-phase thermodynamic contributions to the single-point solution phase energies. Relative Gibbs free energies are reported in kcal mol^{-1} and were converted to 1 M standard state by addition of 1.89 kcal mol^{-1} to all species (according to $RT\ln(c/c_0)$ at 298 K). Relative enthalpies are presented in parenthesis. All energies are quoted relative to the energy of **3a**, and the following nomenclature will be used in the discussion: ΔG relative energy with respect to **3a**; $\Delta\Delta G$ difference between relative energies; $\Delta G^{\ddagger}$ activation energies; and $\Delta\Delta G^{\ddagger}$ difference between activation energies. The fully detailed energy profiles inclusive of all the intermediates not presented in the text are presented in the ESI.† All calculations were performed by using the Gaussian09 package, revision D.01.[31] Figures were created with CLYview[32] and all H atoms were omitted for clarity except for the H atoms involved in the C–H bond activation process. Root-mean-square deviation (RMSD) of atomic positions values were calculated using ICM Molsoft Browser Software. Representative geometrical parameters are also reported (Å, degrees).

Results and discussion

Oxidative addition and intramolecular carbopalladation steps

Our investigation started by the computational analysis of the initial steps of the reaction, namely the oxidative addition and the intramolecular carbopalladation steps (Fig. 2).

Coordination of the palladium catalyst to the aromatic ring of **3a** provides intermediate **4** (ΔG = +5.0 kcal mol^{-1}) which undergoes an oxidative addition process to generate **5** (ΔG = −18.6 kcal mol^{-1}). This step requires only 6.6 kcal mol^{-1} and

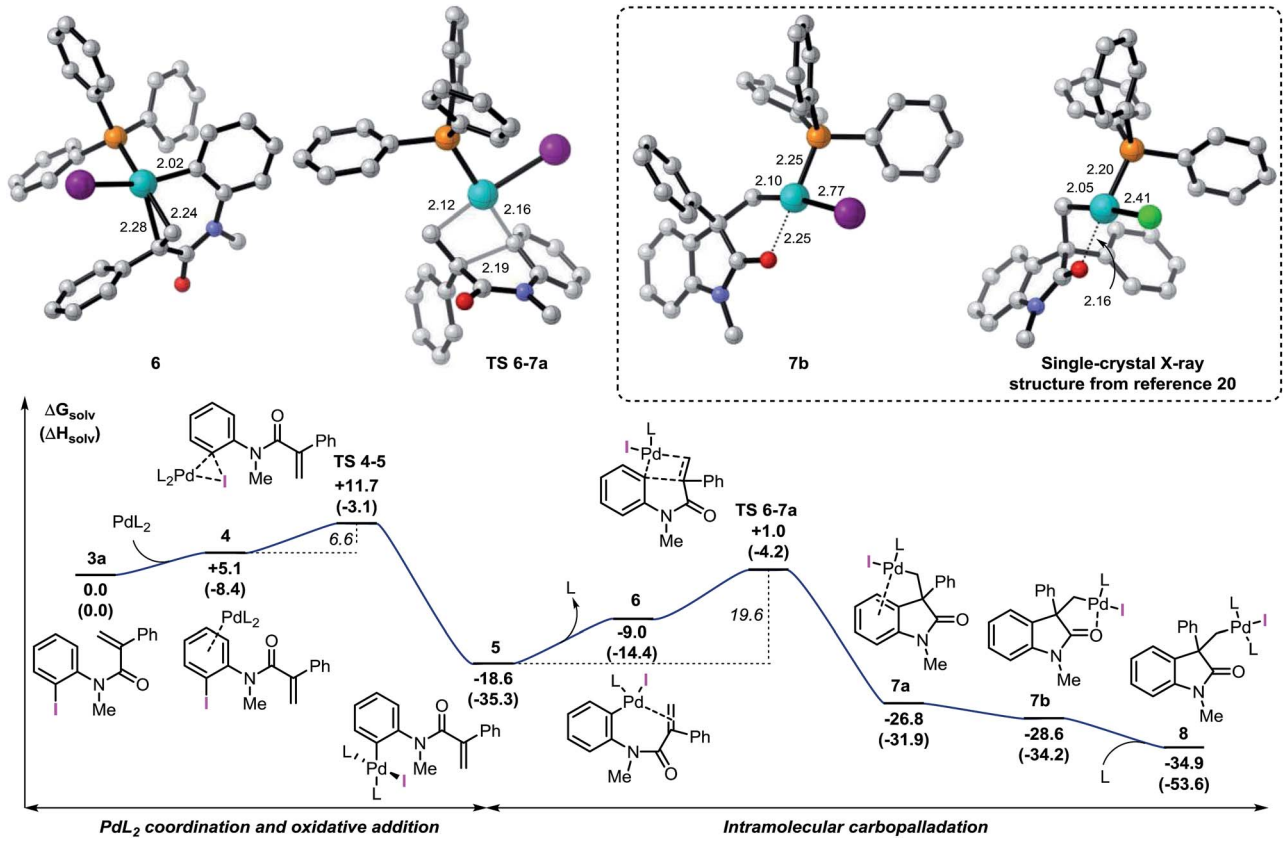

Fig. 2 Free energy profile for the oxidative addition and intramolecular carbopalladation steps and selected computed structures (L = Ph_3P). Comparison between the computed structure for intermediate **7b** and the related single-crystal X-ray structure from ref. 20.

the two intermediates are connected by **TS 4–5** (ΔG = +11.7 kcal mol^{-1}), which models a concerted three-membered process. In 2006, Norrby and co-workers reported a detailed computational study on the oxidative addition of triphenylphosphine–palladium complexes to haloarenes.[33a] The authors found that low-coordinated palladium species such as [Pd(Ph_3P)S], where S is a molecule of a coordinating solvent, would be more reactive than palladium complexes with two or more phosphine ligands. Furthermore, Vidossich *et al.* studied by means of explicit solvent molecular dynamic simulation the equilibration of [Pd(Ph_3P)$_n$S$_m$] species in toluene suggesting that a bare [Pd(Ph_3P)] promptly coordinates to a molecule of solvent.[33d] Attempts to locate a transition state analogous to **TS 4–5** where only one ligand is placed on the metal center were unsuccessful in our case. The results obtained in this analysis suggest that the potential energy surface for the oxidative addition step of a [Pd(Ph_3P)] species to substrate **3a** would be particularly flat in a non-coordinating solvent such as toluene. Although this circumstance renders the search of transition states particularly challenging, it also suggests that a monoligated palladium catalyst may indeed provide a lower energy pathway for this step.

Decoordination of one ligand in **5**, provides an empty coordination site on palladium that allows the interaction with the tethered alkene to generate intermediate **6** (ΔG = −9.0 kcal mol^{-1}) with an overall destabilization of 9.6 kcal mol^{-1}. Intramolecular migratory insertion of the unsaturated moiety into the Pd–C bond leads to intermediate **7a** (ΔG = −26.8 kcal mol^{-1}) where the metal center coordinates to the fused aromatic ring of the newly formed oxindole core. The overall process requires 19.6 kcal mol^{-1} and is modeled by **TS 6–7a** (ΔG = +1.0 kcal mol^{-1}).

Among the different conformers of **7a**, a lower energy structure **7b** (ΔG = −28.6 kcal mol^{-1}) was found where the palladium atom coordinates to the oxygen atom of the carbonyl functionality. Of note, this structure closely resembles the X-ray structure previously reported (Fig. 2).[20] In order to compare the

Table 1 Comparison of the key geometrical parameters for **7b**, **7b-Cl** and the single-crystal X-ray structure from ref. 20

	7b	7b-Cl	X-ray
Pd–X	2.770	2.469	2.408
Pd–P	2.252	2.248	2.196
Pd–O	2.247	2.249	2.162
Pd–C	2.097	2.083	2.050
C–Pd–O	81.0	81.0	81.7
O–Pd–X	89.4	91.1	92.5
X–Pd–P	95.4	92.7	91.0
P–Pd–C	94.1	95.0	95.0
L–Pd–O	174.8	175.6	173.1
C–Pd–X	169.9	171.8	173.8

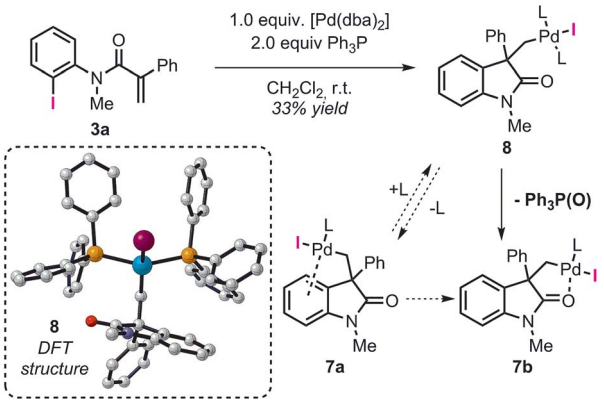

Scheme 3 NMR studies on the equilibration between **7a**, **7b**, and **8** from ref. 20 (L = Ph_3P). Computed structure for intermediate **8**.

geometrical features of these structures, the structure of intermediate **7b-Cl** was optimized after replacement of the iodine atom in **7b** with a chlorine atom (see ESI†). Key bond distances and bond angles in these structures are presented in Table 1. Comparison of the bond distances between the metal atom and the four ligands in the reported X-ray crystal structure and the optimized intermediate **7b-Cl** provides a mean standard deviation (SD) of 0.061 Å. These bond distances are expected to be only marginally influenced by solid-state packing effects thus highlighting the accuracy of the BP86/6-31G(d,p) method used in geometry optimizations. Aware that these solid-state packing effects could significantly affect the torsion angles of the phosphine ligand and of the phenyl moiety, we found that the root-mean-square deviation (RMSD) of atomic positions between the two structures still provides a remarkable correlation with a value of 0.760 Å (see ESI†).[34] Coordination of a phosphine ligand in **7b** gives the more stable bis-ligated intermediate **8** ($\Delta G = -34.9$ kcal mol^{-1}). This complex is characterized by a distorted square planar geometry around the metal center (P–Pd–P = 148.5; C–Pd–I = 157.2) due to the steric hindrance of the two ligands in trans relative arrangement and the iodine atom. The equilibration between **7a**, **7b**, and **8** in solution has been previously studied by means of ^{1}H NMR techniques (Scheme 3).[20] A solution of **8**, prepared by independent synthesis, in deuterated chloroform at room temperature was analyzed by ^{1}H NMR at different times. After the initial formation of a new species, tentatively attributed to intermediate **7a**, significant formation of **7b** with concomitant generation of triphenylphosphine oxide was observed (no free phosphine was detectable after 11 h). These experimental results seem to be in discordance with our computational study, where the bis-ligated complex **8** is thermodynamically more stable than **7a** and **7b**. A closer analysis of the data obtained in this ^{1}H NMR study reveals that after 5 h, a substantial amount of triphenylphosphine oxide is formed and its concentration

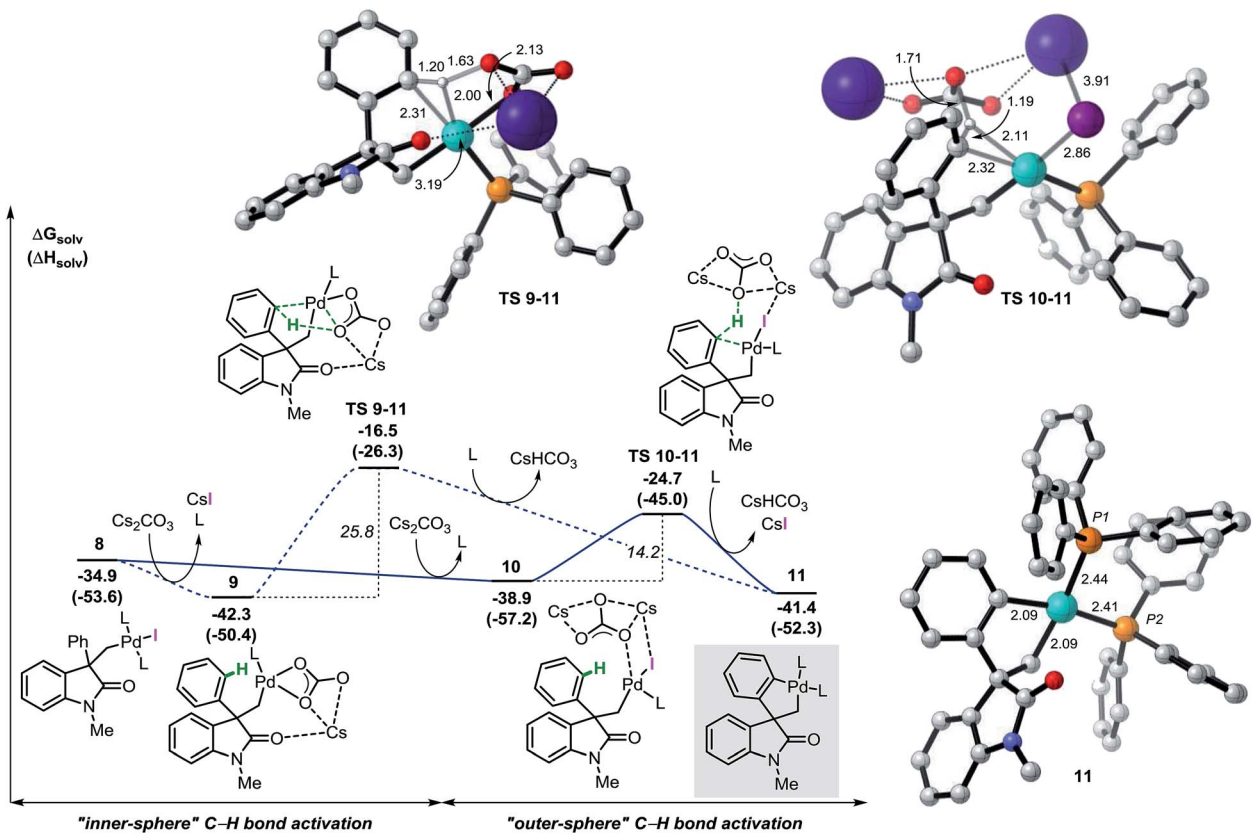

Fig. 3 Free energy profiles of the alternative pathways for the base mediated C–H bond activation step and selected computed structures (L = Ph_3P).

Table 2 Comparison of the key geometrical parameters for spirocyclic palladacycle **11**: computed structure and single-crystal X-ray structure from **14**

	11 (DFT)	**11** (X-ray)
Pd–C(sp^3)	2.098	2.076
Pd–C(sp^2)	2.095	2.076
Pd–P1	2.438	2.358
Pd–P2	2.414	2.335
C(sp^2)–Pd–P2	93.6	92.1
P2–Pd–P1	98.9	97.0
P1–Pd–C(sp^3)	90.2	91.2
C(sp^2)–Pd–C(sp^3)	77.5	79.9
C(sp^2)–Pd–P2	167.2	170.2
C(sp^3)–Pd–P1	169.8	171.4

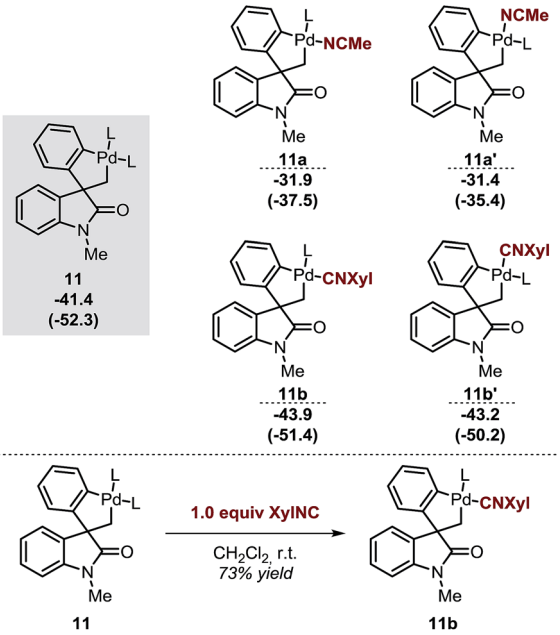

Scheme 4 Relative energies of different analogues of **11** after replacement of a ligand by a solvent molecule (top, L = Ph_3P) and experimental result from ref. 20 (bottom).

increases over time along with formation of **7b**. The irreversible formation of triphenylphosphine oxide would reduce the concentration of free ligand in solution, thus providing the necessary thermodynamic driving force for the formation of the higher energy intermediate **7b** instead of the more stable bis-ligated intermediate **8**.

C–H bond activation step and formation of the spirocyclic palladacycle intermediate

The analysis of the potential energy surface for the base mediated C–H bond activation step provides two possible pathways (Fig. 3). In the first scenario, ligand exchange on intermediate **8** generates the carbonate complex **9** ($\Delta G = -42.3$ kcal mol^{-1}). A subsequent concerted *inner*-sphere metallation deprotonation mechanism could occur generating the corresponding spirocyclic complex **11** ($\Delta G = -41.4$ kcal mol^{-1}).[35] This process requires 25.8 kcal mol^{-1} and it is modeled by **TS 9–11** ($\Delta G = -16.5$ kcal mol^{-1}). This transition state is characterized by a shortening of the Pd–C(sp^2) distance and concomitant abstraction of the hydrogen atom by the carbonate base bound to the metal center. Furthermore, during this process, the large cesium ion interacts with the oxygen atom in the carbonyl group of the oxindole ring (for other examples in which the cation is included in the transitions state for C–H activation processes, see ref. 36). An alternative pathway for the formation of palladacycle **11** was computed. Interaction between the carbonate base and **8** generates intermediate **10** ($\Delta G = -38.9$ kcal mol^{-1}) where the iodine ligand still binds to the metal center. A concerted *outer*-sphere metallation deprotonation mechanism follows and requires 14.2 kcal mol^{-1}. The corresponding transition state **TS 10–11** ($\Delta G = -24.7$ kcal mol^{-1}) models the formation of the Pd–C(sp^2) bond with concomitant abstraction of the hydrogen atom by the carbonate base that does not directly interact with the palladium atom. Agostic-type structures with pre-coordination of the C(sp^2)–H bond to the metal center prior to the C–H bond activation were not observed either by conformational search nor by IRC/QRC calculations. This type of interaction has been proposed to polarize the C–H bond, thus facilitating the deprotonation step and has been found in related computational studies.[36] The overall results shown in Fig. 3 suggest that a base mediated concerted *outer*-sphere metallation deprotonation mechanism is thermodynamically ($\Delta\Delta G = -8.2$ kcal mol^{-1}) and kinetically ($\Delta\Delta G^{\ddagger} = -11.6$ kcal mol^{-1}) favored over the previously reported *inner*-sphere type pathway for this type of reaction.[12] These computational results are further corroborated by a number of experimental results. In the development of a palladium-catalyzed spirocyclization reaction based on a C(sp^2)–H bond activation and benzyne migratory insertion sequence, our groups independently demonstrated that CsF, a salt that is used for the *in situ* generation of aryne reactants, is an effective replacement of Cs_2CO_3 as a base in this reaction. Since fluoride ions would not be able to coordinate to the metal center and promote hydrogen abstraction, this observation suggests the viability of an *outer*-sphere type C–H bond activation process in our system. The feasibility of such process is also computationally supported by the successful optimization of a transition state resembling the structural features of **TS 10–11** where the carbonate base was replaced with CsF (see ESI†). Furthermore, we found that replacement of the hydrogen atoms in the non-halogenated phenyl ring of **3a** with deuterium does not provide any measurable kinetic isotope effect (KIE),[14] which suggests that C–H bond activation is not the rate-limiting step in the catalytic cycle. Since the subsequent insertion of arynes is a fast process (*vide infra*), the absence of a KIE is not compatible with the highly energy demanding *inner*-sphere type C–H bond activation mechanism ($\Delta G^{\ddagger} = 25.8$ kcal mol^{-1}) thus supporting the alternative *outer*-sphere type mechanism ($\Delta G^{\ddagger} = 14.2$ kcal mol^{-1}).

The spirocyclic palladacycle **11** ($\Delta G = -41.4$ kcal mol^{-1}) is characterized by a distorted square planar geometry around the metal center due to the *cis* arrangement of the two phosphine ligands. We previously reported the synthesis and

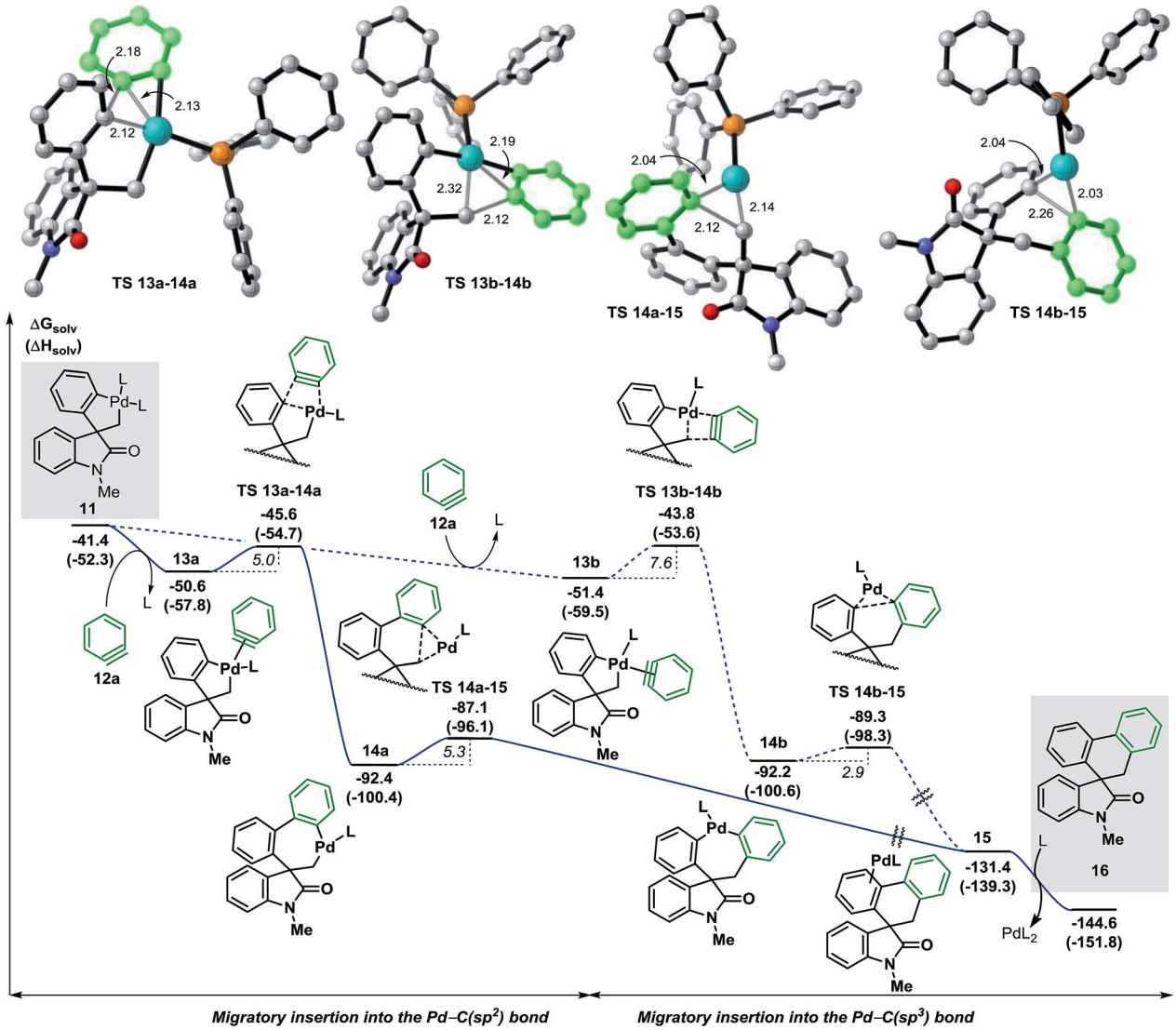

Fig. 4 Free energy profile for the migratory insertion step with benzyne **12a** and transition state structures (L = Ph_3P).

characterization of **11**, and demonstrated the viability of this intermediate in this class of reactions.[14,16] Table 2 summarizes the key structural features of the computed and the single-crystal X-ray structure of **11**. In analogy to the case of intermediate **7b-Cl**, there is a remarkable similarity in both the key Pd–R distances, with a SD of 0.058 Å, and in the overall structure with a RMSD of 0.375 Å (see ESI†). Decoordination of a ligand *trans* to either the C(sp^2) or the C(sp^3) atoms in **11** provides a significant increase in energy of the resulting 14-electron complexes (ΔG = −26.1 and −26.6 kcal mol^{-1}, respectively). Since the spirocyclization reaction of aryne substrates is carried out in a toluene/acetonitrile mixture,[13,14] we envisioned that replacement of a phosphine ligand in **11** by coordination a molecule of MeCN would be possible (Scheme 4, top). The relative energies of the resulting intermediates **11a** and **11a′** show higher energy species in both cases (ΔG = −31.9 and −31.4 kcal mol^{-1}, respectively) with a slight preference for the substitution of the phosphine ligand *trans* of the C(sp^2)–Pd bond. Attempts to detect these type of intermediates by ^{1}H NMR analysis of a solution of **11** in MeCN-d_3 were inconclusive. However, treatment of **11** with one equivalent of xylylisocyanide (XylNC) provides a single isomeric species that was attributed to **11b** (Scheme 4, bottom).[20] Indeed, replacement of a phosphine ligand with a XylNC molecule provides the two more stable structures **11b** and **11b′** (ΔG = −43.9 and −43.2 kcal mol^{-1}, respectively) being **11b** thermodynamically favored with respect to **11b′** and the original palladacycle **11**.

Regioselectivity of the migratory insertion step

We next studied the migratory insertion step in the spirocyclic palladacycle intermediate **11** for the case of benzyne **12a** (Fig. 4). According to the general mechanism presented in Fig. 1, a ligand substitution on **11** could generate either **13a** or **13b** (ΔG = −50.6 and −51.4 kcal mol^{-1}, respectively). In **13a** the benzyne ligand **12a** binds to the metal center in a *trans* position with respect to the C(sp^3) atom whereas in **13b** it binds in *trans* to the

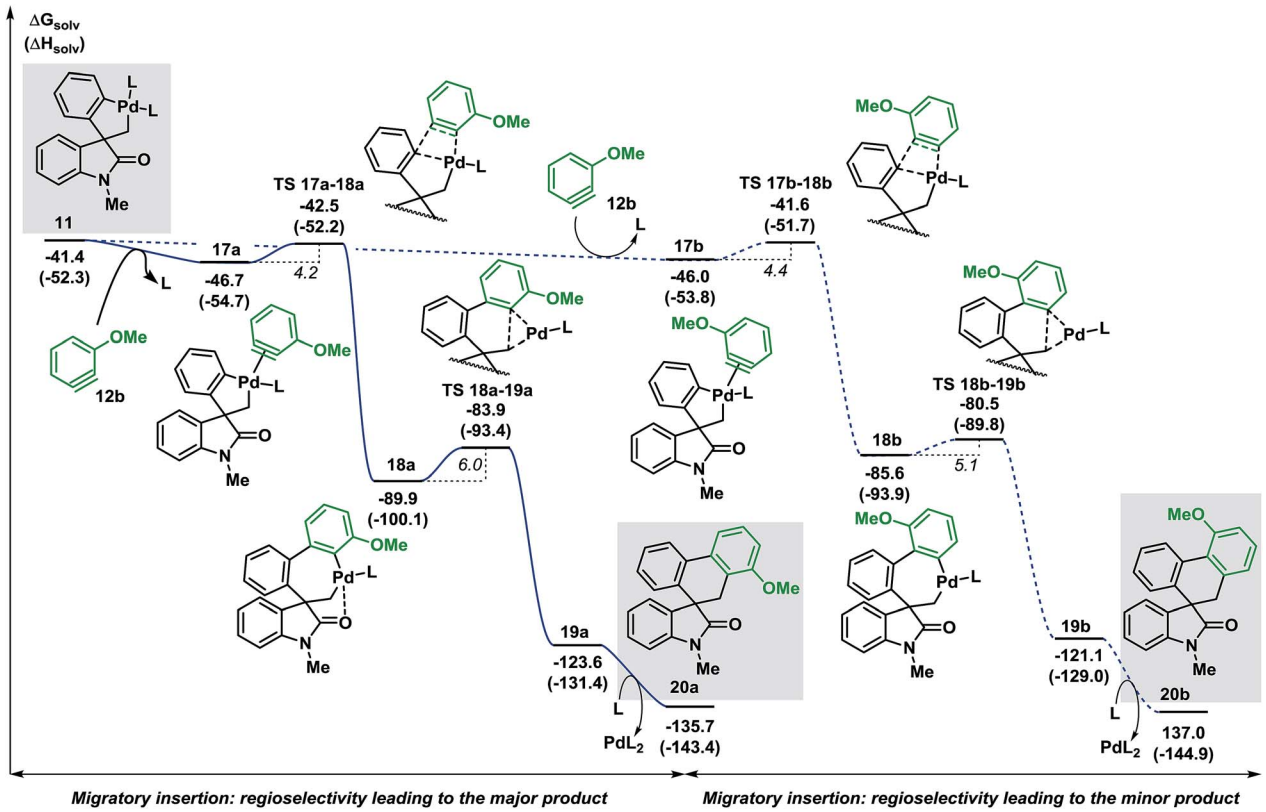

Fig. 5 Computed Gibbs free energy profile explaining the regioselectivity of the migratory insertion of 3-methoxy substituted benzyne **12b** (L = Ph_3P).

C(sp^2) atom. Although the formation of **13b** is slightly favored thermodynamically ($\Delta\Delta G = -0.8$ kcal mol^{-1}) the subsequent migratory insertion step is kinetically favored for intermediate **13a** ($\Delta\Delta G^{\ddagger} = -1.8$ kcal mol^{-1}) following a classic Curtin-Hammet scenario.[37] This trend is maintained in all the cases presented in this work, therefore, only the profiles involving migratory insertions into the Pd–C(sp^2) bond of **11** will be discussed here (see ESI† for the profiles of selected cases of migratory insertions into the Pd–C(sp^3) bond). The corresponding transition states **TS 13a–14a** ($\Delta G = -45.6$ kcal mol^{-1}) and **TS 13b–14b** ($\Delta G = -43.8$ kcal mol^{-1}) model a planarization of the benzyne ring with respect to the phenyl moiety during the formation of the C(sp^2)–(Csp^2) and the C(sp^2)–(Csp^3) bonds, respectively. The two isomers **14a** and **14b** ($\Delta G = -92.4$ and -92.2 kcal mol^{-1}, respectively) are characterized by a remarkable thermodynamic stability and to be almost isoenergetic. The geometry of these intermediates facilitates the subsequent C–C bond-forming reductive elimination process ($\Delta G^{\ddagger} = 5.3$ and 2.9 kcal mol^{-1}, respectively). Transition states **TS 14a–15** and **TS 14b–15** ($\Delta G = -87.1$ and -89.3 kcal mol^{-1}, respectively) model a shortening of the C(sp^2)–(Csp^3) and C(sp^2)–(Csp^2) distances, respectively, and the concomitant migration of the palladium atom on the adjacent π-aromatic system to form the spirooxindole complex **15** ($\Delta G = -131.4$ kcal mol^{-1}). Final ligand-assisted decoordination of the catalyst releases the final product **16** ($\Delta G = -144.6$ kcal mol^{-1}) and regenerates the [$Pd(Ph_3P)_2$] active catalyst. In an attempt to isolate or detect any intermediate **13–15** in the reaction mixture, preformed palladacycle **11** was treated with benzyne generated *in situ* at room temperature but only product **16** was detected.[20] In agreement with this experiment, the low activation energies and the remarkable exergonic nature for the migratory insertion and the C–C bond-forming reductive elimination steps suggest that the concentration of any of the unstable intermediates **13–15** would be extremely low in catalytic and stoichiometric conditions.

Evaluation of the potential energy surface for the migratory insertion of the unsymmetrical 3-methoxy substituted benzyne **12b** is presented in Fig. 5. In this case, the unsymmetrical aryne

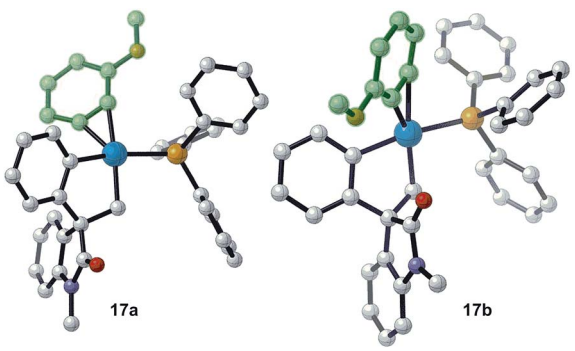

Fig. 6 Computed structure for intermediates **17a** and **17b** highlighting the different orientations of the methoxy substituent.

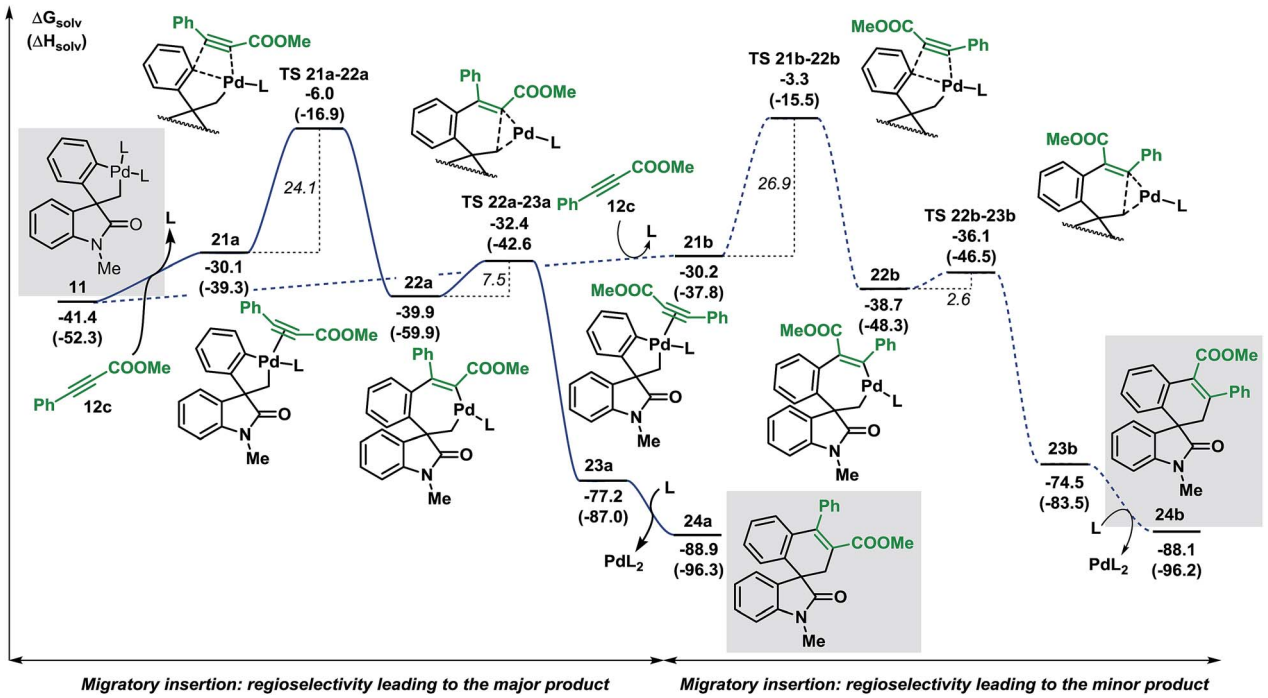

Fig. 7 Computed Gibbs free energy profile explaining the regioselectivity of the migratory insertion of methyl 3-phenylpropiolate **12c** (L = Ph_3P).

12b introduces a new regioselective element, based on the different relative positions of the methoxy substituent with respect to the spirocyclic core of the oxindole moiety. Coordination of **12b** to **11** generates either **17a** ($\Delta G = -46.7$ kcal mol^{-1}) or **17b** ($\Delta G = -46.0$ kcal mol^{-1}). The methoxy group in intermediate **17a** points toward the phosphine ligand whereas in **17b** this substituent points toward the oxindole backbone (Fig. 6).

In analogy to **12a**, insertion of the substituted aryne in **17a** and **17b** is a fast process ($\Delta G^{\ddagger} = 4.2$ and 4.4 kcal mol^{-1}, respectively). The relative energy of the corresponding transition states **TS 17a–18a** and **TS 17b–18b** ($\Delta G = -42.5$ and -41.6 kcal mol^{-1}, respectively) favors the formation of **18a** ($\Delta G = -89.9$ kcal mol^{-1}) over **18b** ($\Delta G = -85.6$ kcal mol^{-1}). Subsequent C(sp^2)–C(sp^3) bond-forming reductive elimination proceeds *via* **TS 18a–19a** and **TS 18b–19b** ($\Delta G = -83.9$ and -80.5 kcal mol^{-1}, respectively) to generate the two isomeric complexes **19a** and **19b** ($\Delta G = -123.6$ and -121.1 kcal mol^{-1}, respectively). Decoordination of the catalyst ultimately releases the two compounds **20a** and **20b** ($\Delta G = -135.7$ and -137.0 kcal mol^{-1}, respectively). The reaction between **3a** and 3-methoxy benzyne **12b** carried out under the standard reaction conditions[14] affords the desired spirooxindoles products **20a** and **20b** in a mixture 3 : 1 (see ESI†). The experimental ratio (3 : 1) is in good agreement with the calculated theoretical ratio ($\Delta\Delta G = 0.9$ kcal mol^{-1}, corresponding to a 3.6 : 1 ratio at 80 °C) in favor of the same isomer **20a**.[38]

Reactivity and regioselectivity for the migratory insertion of alkynes

In order to examine the regioselectivity of the reaction with other unsaturated compounds, we selected less reactive π-systems such as unsymmetrical internal alkynes.[16] Indeed, minor adjustments of the reaction conditions allowed the generation of the desired spirocyclic products in excellent

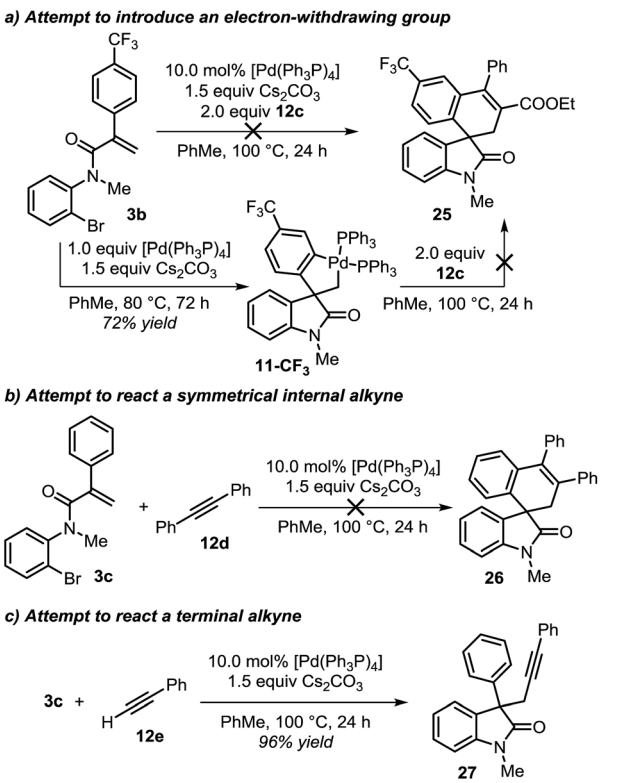

Scheme 5 Attempts for the insertion of alkyne reactants.

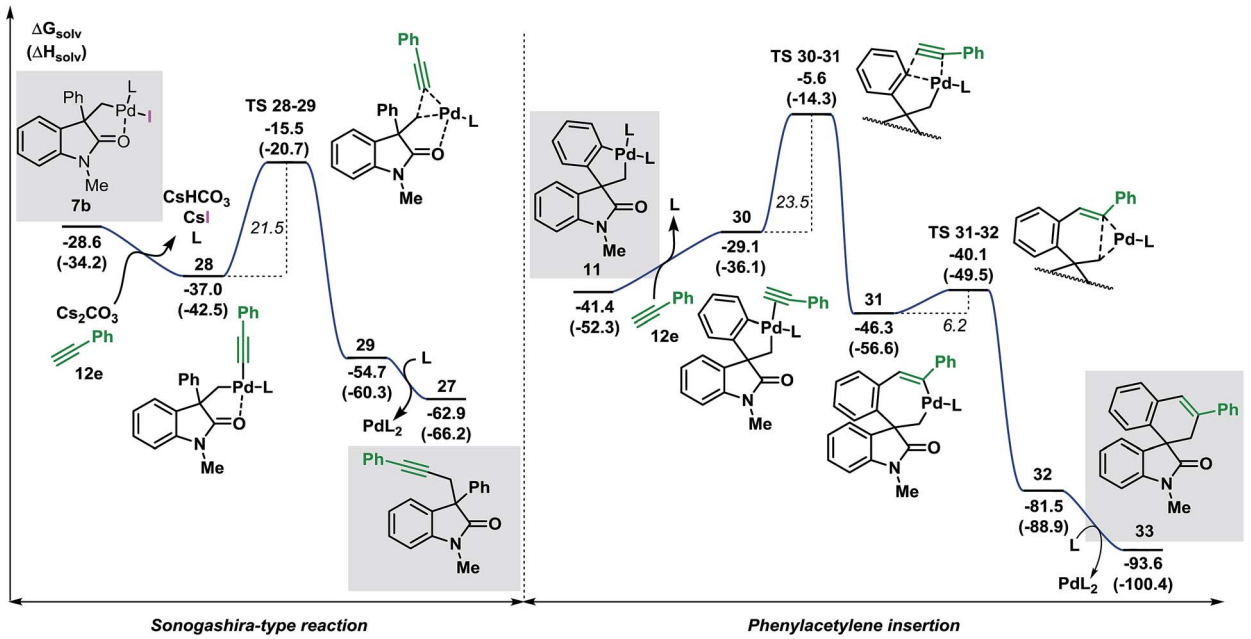

Fig. 8 Comparison between the free energy profiles for the Sonogashira-type reaction (left side) and the migratory insertion reaction (right side) with terminal alkyne **12e** (L = Ph_3P).

regioselectivity (>20 : 1). The computational analysis of the migratory insertion step for methyl 3-phenylpropiolate **12c** is presented in Fig. 7.[39]

Coordination of the alkyne **12c** to the palladium atom in **11** provides the two isomeric structures **21a** and **21b** ($\Delta G = -30.1$ and -30.2 kcal mol^{-1}, respectively). Migratory insertion takes place and the formation of a new C(sp^2)–C(sp^2) bond is modeled by transition states **TS 21a–22a** and **TS 21b–22b** ($\Delta G = -6.0$ and -3.3 kcal mol^{-1}, respectively) to generate intermediates **22a** and **22b** ($\Delta G = -39.9$ and -38.7 kcal mol^{-1}, respectively). The energies required for these insertion processes ($\Delta G^{\ddagger} = 24.1$ and 26.9 kcal mol^{-1}, respectively) are significantly higher (>15 kcal mol^{-1}) than the activation energies calculated in the case of arynes. This result reflects the higher temperatures required for the insertion of internal alkynes compared to arynes (100 °C *vs.* 80 °C). The following C(sp^2)–C(sp^3) bond-forming reductive elimination step is modeled by **TS 22a–23a** and **TS 22b–23b** ($\Delta G = -32.4$ and -36.1 kcal mol^{-1}, respectively) and requires 7.5 and 2.6 kcal mol^{-1}, respectively. Final decoordination of the palladium complex from intermediates **23a** and **23b** ($\Delta G = -77.2$ and -74.5 kcal mol^{-1}, respectively) releases the corresponding products **24a** and **24b** ($\Delta G = -88.9$ and -88.1 kcal mol^{-1}, respectively). Of note, the kinetic theoretical ratio of **24a** and **24b** at 100 °C is 38 : 1, a value in good agreement with the ratios obtained experimentally (>20 : 1).

During the evaluation of the scope of this transformation, we found that introduction of an electron-withdrawing group on the pendant aromatic ring failed to generate the corresponding spirooxindole product **25** (Scheme 5a).[16]

Furthermore, when palladacycle **11-CF_3** was successfully synthesized by independent synthesis, its reaction with internal alkyne **12d** did not generate the expected product **26**. Analysis of the alkyne migratory insertion step in complex **11-CF_3** provides an activation energy only 2.6 kcal mol^{-1} higher than for the insertion in **21a** (see ESI†). These results and experimental observations suggest that the low stability of complex **11-CF_3** under the reaction conditions, in combination with a slower migratory insertion step, could be responsible for the lack of product formation. In other experiments, we found that the reaction of internal symmetrical alkynes such as **12d** did not generate the expected product **26** (Scheme 5b).[16] The energetics of the migratory insertion step for alkyne **12d** was evaluated (see ESI†). The computed activation energy ($\Delta G^{\ddagger} = 32.2$ kcal mol^{-1}) is 8.1 kcal mol^{-1} higher than for the insertion of unsymmetrical alkyne **12c** ($\Delta G^{\ddagger} = 24.1$ kcal mol^{-1}) supporting a particularly slow insertion step. The anticipated low rate for this insertion process, along with the kinetic stability of the active catalyst, may explain the lack of product formation in this case. In addition to these experiments, in an attempt to react substrate **3c** with phenylacetylene **12e**, we observed exclusive formation of the known compound **27** instead of the expected spirocyclic product (Scheme 5c). The computational analysis for the formation of this Sonogashira-type compound **27** is shown in Fig. 8.

The base present in the reaction media facilitates a ligand exchange process in intermediate **7b** to generate the organometallic species **28** ($\Delta G = -37.0$ kcal mol^{-1}).[40] Ensuing C(sp^3)–(Csp) bond-forming reductive elimination generates intermediate **29** ($\Delta G = -54.7$ kcal mol^{-1}) where the palladium atom coordinates to the alkyne moiety. This step requires 21.5 kcal mol^{-1} and is modeled by **TS 28–29** ($\Delta G = -15.5$ kcal mol^{-1}). Interaction between the oxygen atom of the carbonyl functionality and the metal center was observed during the whole transformation. Decoordination of the

Table 3 Experimental studies on the alternative migratory insertion/C–H bond activation pathway

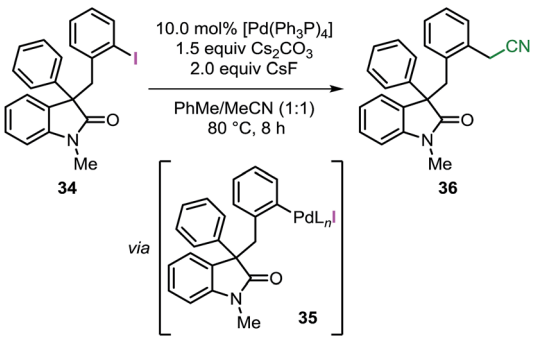

Entry	Variations from the standard conditions	Yield
1	None	52%
2	PhMe instead of PhMe/MeCN (1 : 1)	0%
3	No $[Pd(Ph_3P)_4]$	0%
4	No Cs_2CO_3/CsF	0%

catalyst releases the final product **27** ($\Delta G = -62.9$ kcal mol^{-1}). The alternative migratory insertion pathway starts with a ligand exchange process on palladacycle **11** to form intermediate **30** ($\Delta G = -29.1$ kcal mol^{-1}). Insertion of the alkyne ligand into the C(sp^2)–Pd bond requires 23.5 kcal mol^{-1} and the corresponding transition state **TS 30–31** ($\Delta G = -5.6$ kcal mol^{-1}) connects **30** to the resulting seven-membered palladacycle **31** ($\Delta G = -46.3$ kcal mol^{-1}). Final C(sp^2)–C(sp^3) bond-forming reductive elimination is modeled by **TS 31–32** ($\Delta G = -40.1$ kcal mol^{-1}) and, upon decoordination of the catalyst, generates the expected product **33** ($\Delta G = -93.6$ kcal mol^{-1}). Comparison between the two possible pathways shows that the Sonogashira-type reaction on intermediate **7b** is kinetically and thermodynamically favoured over the anticipated migratory insertion process ($\Delta\Delta G^{\ddagger} = -2.0$ kcal mol^{-1} and $\Delta\Delta G = -9.9$ kcal mol^{-1}, respectively). This result is in agreement with the experimental data where the reaction between **3c** and the terminal alkyne **12e** under the standard reaction conditions provides product **27** exclusively.

Experimental studies on the alternative migratory insertion/C–H bond activation sequence

As mentioned in the introduction, intermediate **C** in Fig. 1 may undergo migratory insertion with the unsaturated reactant prior to the C–H bond activation step. In order to establish the feasibility of this sequence, substrate **34** was independently synthesized and submitted to the standard reaction conditions (Table 3). Oxidative addition of the low-valent catalyst into the reactive C(sp^2)–I bond would generate intermediate **35** (analogous to intermediate **J** in Fig. 1).[41] In the presence of a base, **35** could undergo intramolecular C–H bond activation on the unsubstituted phenyl ring to eventually form the spirooxindole **16**, corresponding to the product obtained for the reaction of **3a** with a benzyne precursor. Unexpectedly, the reaction of **34** provided compound **36** exclusively with the remaining mass balance represented by unreacted starting material (Table 3, entry 1). Product **36** presumably derives from the reaction between intermediate **35** (generated *in situ*) and the acetonitrile co-solvent. Indeed, the reaction carried out in pure toluene did not afford any product but only full recovery of starting material (Table 3, entry 2). Exclusion of either the palladium catalyst or the base also resulted in unreacted starting material (Table 3, entry 3 and 4). Of note, compound **36** has never been detected in

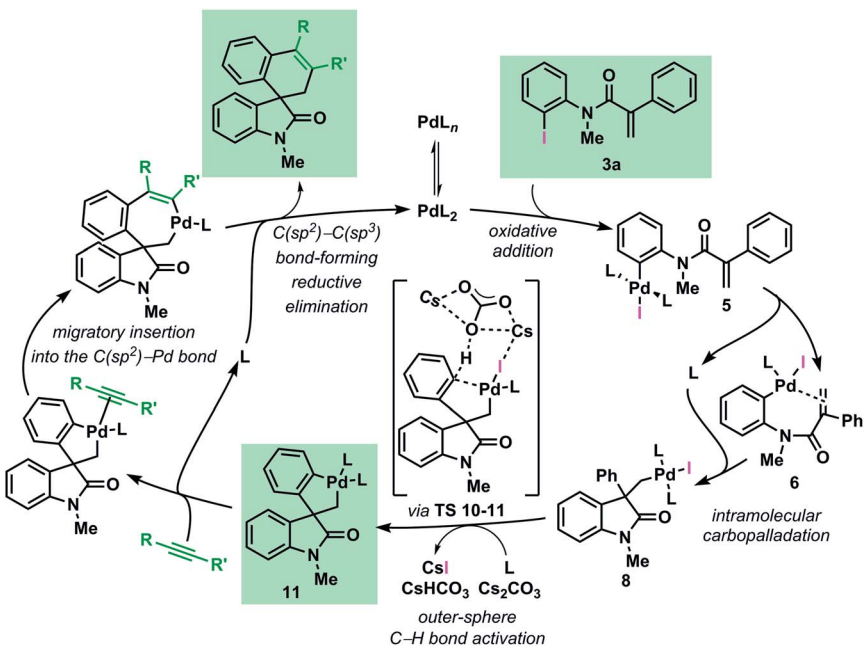

Fig. 9 Catalytic cycle for the computed most favourable pathway for the Pd-catalyzed spirocyclization reaction (L = Ph_3P).

any catalytic reaction during the optimization or the evaluation of scope of the spirocyclization reaction with arynes.[14] These collective observations suggest that the alternative pathway initially proposed, where migratory insertion take places before the C–H bond activation step, is unlikely to be operative in the system under study. Unfortunately, attempts to carry out a computational analysis for this alternative mechanism provided a scenario inconsistent with the experimental results (see ESI†).

Conclusions

The mechanism of the palladium-catalyzed spirocyclization of acrylamides with arynes and alkynes has been investigated by means of density functional theory calculations coupled with experimental studies. Our results show an excellent agreement between theoretical and experimental data and support the initially postulated mechanism for this reaction proceeding *via* a C–H bond activation and migratory insertion sequence. The most favorable pathway, based on the results of this study, is presented in Fig. 9.

Investigation of the early stages of the reaction supports the existence of several species in equilibrium and comparisons between the computed and the single-crystal X-ray structures of some of these intermediates show a remarkable similarity. The intramolecular migratory insertion was found to be the rate determining step in the formation of the palladacycle intermediate **11**. The C–H bond activation step is found to proceed *via* a concerted *outer*-sphere metallation deprotonation mechanism. This scenario is supported by kinetic measurements and by evaluation of other bases. Furthermore, ligand dissociation and exchange in the experimentally isolated palladacycle **11** was studied. The analysis of the migratory insertion step revealed that the process is consistently favored for the insertion into the C(sp^2)–Pd bond in all the cases and it originates the observed stereoselectivities *via* kinetic control. The differences in the energies obtained in the case of aryne and alkyne reactants correlate to the different sets of experimental conditions. Furthermore, the calculated regioselectivities for the insertion of unsymmetrical unsaturated reactants are in excellent agreement with the experimental ratio previously reported. Finally, experimental data provide evidence that the alternative mechanism where the migratory insertion process precedes the C–H activation step is not operative under the standard reaction conditions.

Conflicts of interest

The authors declare no conflict of interests.

Acknowledgements

We are grateful for financial support from the Natural Sciences and Engineering Research Council (NSERC), the University of Toronto (U of T), the University of Geneva (U of G) and Alphora Research Inc. I. F. thanks the Collaborative Research and Training Experience (Create ChemNET) program for a postdoctoral fellowship. H. Y. thanks the Ontario Graduate Scholarship (OGS) program for funding. We thank Dr Marcus Wegmann (U of T), Nicolas Zeidan (U of T), José F. Rodríguez (U of T), and Egor Larin (U of T) for proofreading the manuscript and for discussions. We thank Dr Marco van Woerden (Van Woerden Consultancy) for the preparation of Python scripts used for data analysis. We also thank Carmine Chiancone (U of G) for technical support.

Notes and references

1 For selected reviews and references therein, see: (*a*) F. Shi and R. C. Larock, in *C–H Activation*, ed. J.-Q. Yu and Z. Shi, Springer, Heidelberg, 2010, pp. 123–164; (*b*) R. Giri, B.-F. Shi, K. M. Engle, N. Maugel and J.-Q. Yu, *Chem. Soc. Rev.*, 2009, **38**, 3242; (*c*) T. W. Lyons and M. S. Sanford, *Chem. Rev.*, 2010, **110**, 1147; (*d*) O. Baudoin, *Chem. Soc. Rev.*, 2011, **40**, 4902; (*e*) T. Gensch, M. N. Hopkinson, F. Glorius and J. Wencel-Delord, *Chem. Soc. Rev.*, 2016, **45**, 2900; (*f*) H. M. L. Davies and D. Morton, *J. Org. Chem.*, 2016, **81**, 343; (*g*) J. F. Hartwig, *J. Am. Chem. Soc.*, 2016, **138**, 2; (*h*) X.-S. Xue, P. Ji, B. Zhou and J.-P. Cheng, *Chem. Rev.*, 2017, **117**, 8622; (*i*) Y. Yang, J. Lan and J. You, *Chem. Rev.*, 2017, **117**, 8787; (*j*) J. R. Hummel, J. A. Boerth and J. A. Ellman, *Chem. Rev.*, 2017, **117**, 9163.

2 For selected reviews and references therein, see: (*a*) K. Godula and D. Sames, *Science*, 2006, **312**, 67; (*b*) D. Alberico, M. E. Scott and M. Lautens, *Chem. Rev.*, 2007, **107**, 174; (*c*) L. McMurray, F. O'Hara and M. J. Gaunt, *Chem. Soc. Rev.*, 2011, **40**, 1885; (*d*) J. Ye and M. Lautens, *Nat. Chem.*, 2015, **7**, 863; (*e*) N. Della Ca', M. Fontana, E. Motti and M. Catellani, *Acc. Chem. Res.*, 2016, **49**, 1389.

3 For selected reviews and references therein, see: (*a*) X. Chen, K. M. Engle, D.-H. Wang and J.-Q. Yu, *Angew. Chem., Int. Ed.*, 2009, **48**, 5094; (*b*) R. Giri, S. Thapa and A. Kafle, *Adv. Synth. Catal.*, 2014, **356**, 1395; (*c*) C. Liu, J. Yuan, M. Gao, S. Tang, W. Li, R. Shi and A. Lei, *Chem. Rev.*, 2015, **115**, 12138; (*d*) Z. Chen, B. Wang, J. Zhang, W. Yu, Z. Liu and Y. Zhang, *Org. Chem. Front.*, 2015, **2**, 1107; (*e*) Y. Park, Y. Kim and S. Chang, *Chem. Rev.*, 2017, **117**, 9247.

4 For selected examples and references therein, see: (*a*) J. J. Topczewski, P. J. Cabrera, N. I. Saper and M. S. Sanford, *Nature*, 2016, **531**, 220; (*b*) Z. Zhang, K. Tanaka and J.-Q. Yu, *Nature*, 2017, **543**, 538.

5 For selected examples and references therein, see: (*a*) D. Leow, G. Li, T.-S. Mei and J.-Q. Yu, *Nature*, 2012, **486**, 518; (*b*) R.-Y. Tang, G. Li and J.-Q. Yu, *Nature*, 2104, **507**, 215; (*c*) X.-C. Wang, W. Gong, L.-Z. Fang, R.-Y. Zhu, S. Li, K. M. Engle and J.-Q. Yu, *Nature*, 2015, **519**, 334; (*d*) Y. Xu, M. C. Young, C. Wang, D. M. Magness and G. Dong, *Angew. Chem., Int. Ed.*, 2016, **55**, 9084; (*e*) K. Hong, H. Park and J.-Q. Yu, *ACS Catal.*, 2017, **7**, 6938.

6 For selected reviews and references therein, see: (*a*) I. Franzoni and C. Mazet, *Org. Biomol. Chem.*, 2014, **12**, 233; (*b*) R. Sharma, K. Thakur, R. Kumar, I. Kumar and U. Sharma, *Catal. Rev.: Sci. Eng.*, 2015, **57**, 345; (*c*) H. J. Davis and R. J. Phipps, *Chem. Sci.*, 2017, **8**, 864.

7 For selected examples and references therein, see: (*a*) M. Sickert, H. Weinstabl, B. Peters, X. Hou and M. Lautens, *Angew. Chem., Int. Ed.*, 2014, **53**, 5147; (*b*) O. Baudoin, *Acc. Chem. Res.*, 2017, **50**, 1114.

8 For selected reviews and references therein, see: (*a*) J. He, M. Wasa, K. S. L. Chan, Q. Shao and J.-Q. Yu, *Chem. Rev.*, 2017, **117**, 8754; (*b*) V. P. Mehta and J.-A. García-López, *ChemCatChem*, 2017, **9**, 1149.

9 For selected examples, see: (*a*) B. Seashore-Ludlow and P. Somfai, *Org. Lett.*, 2012, **14**, 3858; (*b*) X. Liu, X. Ma, Y. Huang and Z. Gu, *Org. Lett.*, 2013, **15**, 4814; (*c*) Z. Liu, Y. Xia, S. Zhou, L. Wang, Y. Zhang and J. Wang, *Org. Lett.*, 2013, **15**, 5032; (*d*) M.-B. Zhou, X.-C. Huang, Y.-Y. Liu, R.-J. Song and J.-H. Li, *Chem.–Eur. J.*, 2014, **20**, 1843; (*e*) D. D. Vachhani, H. H. Butani, N. Sharma, U. C. Bhoya, A. K. Shan and E. V. Van der Eycken, *Chem. Commun.*, 2015, **51**, 14862; (*f*) C. Shen, R.-R. Liu, R.-J. Fan, Y.-L. Li, T.-F. Xu, J.-R. Gao and Y.-X. Jia, *J. Am. Chem. Soc.*, 2015, **137**, 4936; (*g*) W. Kong, Q. Wang and J. Zhu, *Angew. Chem., Int. Ed.*, 2016, **55**, 9714; (*h*) H. Yoon, Y. J. Jang and M. Lautens, *Synthesis*, 2016, **48**, 1483; (*i*) D. A. Petrone, M. Kondo, N. Zeidan and M. Lautens, *Chem.–Eur. J.*, 2016, **22**, 5684.

10 (*a*) B. Burns, R. Gridd, V. Santhakumar, V. Sridharan, P. Stevenson and T. Worakum, *Tetrahedron*, 1992, **48**, 7297; (*b*) R. Grigg, J. M. Sansano, V. Santhakumar, V. Sridharan, R. Thangavelanthum, M. Thornton-Pett and D. Wilson, *Tetrahedron*, 1997, **53**, 11803; (*c*) P. Fretwell, R. Grigg, J. M. Sansano, V. Sridharan, S. Sukirthalingam, D. Wilson and J. Redpath, *Tetrahedron*, 2000, **56**, 7525.

11 Q. Huang, A. Fazio, G. Dai, M. A. Campo and R. C. Larock, *J. Am. Chem. Soc.*, 2004, **126**, 7460.

12 J. Ye, Z. Shi, T. Sperger, Y. Yasukawa, C. Kingston, F. Schoenebeck and M. Lautens, *Nat. Chem.*, 2017, **9**, 361.

13 M. Pérez-Gómez and J.-A. García-López, *Angew. Chem., Int. Ed.*, 2016, **55**, 14389.

14 H. Yoon, A. Lossouarn, F. Landau and M. Lautens, *Org. Lett.*, 2016, **18**, 6324.

15 M. Pérez-Gómez, S. Hernández-Ponte, D. Bautista and J.-A. García-López, *Chem. Commun.*, 2017, **53**, 2842.

16 H. Yoon, M. Rölz, F. Landau and M. Lautens, *Angew. Chem., Int. Ed.*, 2017, **56**, 10920.

17 For selected examples, see: (*a*) O. René, D. Lapointe and K. Fagnou, *Org. Lett.*, 2009, **11**, 4560; (*b*) R. T. Ruck, M. A. Huffman, M. M. Kim, M. Shevlin, W. V. Kandur and I. W. Davies, *Angew. Chem., Int. Ed.*, 2008, **47**, 4711; (*c*) Z. Lu, C. Hu, J. Guo, J. Li, Y. Cui and Y. Jia, *Org. Lett.*, 2010, **12**, 480; (*d*) T. Piou, L. Neville and J. Zhu, *Org. Lett.*, 2012, **14**, 3760; (*e*) T. Piou, L. Neville and J. Zhu, *Angew. Chem., Int. Ed.*, 2012, **51**, 11561; (*f*) T. Piou, A. Bunescu, Q. Wang, L. Neville and J. Zhu, *Angew. Chem., Int. Ed.*, 2013, **52**, 12385; (*g*) M. Wang, X. Zhang, Y.-X. Zhuang, Y.-H. Xu and T.-P. Loh, *J. Am. Chem. Soc.*, 2015, **137**, 1341; (*h*) Z.-Y. Gu, C.-G. Liu, S.-Y. Wang and S.-J. Ji, *Org. Lett.*, 2016, **18**, 2379; (*i*) T. Yao and D. He, *Org. Lett.*, 2017, **19**, 842; (*j*) S. Tong, A. Limouni, Q. Wang, M.-X. Wang and J. Zhu, *Angew. Chem., Int. Ed.*, 2017, **56**, 14192; (*k*) C. Shao, Z. Wu, X. Ji, B. Zhou and Y. Zhang, *Chem. Commun.*, 2017, **53**, 10429.

18 (*a*) B. M. Trost and M. K. Brennan, *Synthesis*, 2009, **18**, 3003; (*b*) J. E. M. N. Klein and R. J. K. Taylor, *Eur. J. Org. Chem.*, 2011, 6821; (*c*) G. S. Singh and Z. Y. Desta, *Chem. Rev.*, 2012, **112**, 6104; (*d*) L. K. Smith and I. R. Baxendale, *Org. Biomol. Chem.*, 2015, **13**, 9907; (*e*) W. Kong, Q. Wang and J. Zhu, *J. Am. Chem. Soc.*, 2015, **137**, 16028; (*f*) B. V. S. Reddy, P. N. Nair, A. Antony and N. Srivastava, *Eur. J. Org. Chem.*, 2017, 5484.

19 H. Zheng, Y. Zhu and Y. Shi, *Angew. Chem., Int. Ed.*, 2014, **53**, 11280.

20 M. Pérez-Gómez, L. Navarro, I. Saura-Llamas, D. Bautista, M. Lautens and J.-A. García-López, *Organometallics*, 2017, **36**, 4465.

21 (*a*) J. P. Perdew and W. Yue, *Phys. Rev. B: Condens. Matter Mater. Phys.*, 1986, **33**, 8800; (*b*) J. P. Perdew, *Phys. Rev. B: Condens. Matter Mater. Phys.*, 1986, **33**, 8822; (*c*) A. D. Becke, *Phys. Rev. A: At., Mol., Opt. Phys.*, 1988, **38**, 3098.

22 X. Li and M. J. Frisch, *J. Chem. Theory Comput.*, 2006, **2**, 835.

23 (*a*) T. H. Dunning Jr and P. J. Hay, *Modern Theoretical Chemistry*, ed. H. F. Schaefer III, Plenum, New York, 1997, vol. 3; (*b*) P. J. Hay and W. R. Wadt, *J. Chem. Phys.*, 1985, **82**, 270; (*c*) W. R. Wadt and P. J. Hay, *J. Chem. Phys.*, 1985, **82**, 284; (*d*) P. J. Hay and W. R. Wadt, *J. Chem. Phys.*, 1985, **82**, 299.

24 (*a*) A. D. MacLean and G. S. Chandler, *J. Chem. Phys.*, 1980, **72**, 5639; (*b*) R. Krishnan, J. S. Binkley, R. Seeger and J. A. Pople, *J. Chem. Phys.*, 1980, **72**, 650.

25 (*a*) K. Fukui, *Acc. Chem. Res.*, 1981, **14**, 363; (*b*) H. P. Hratchian and H. B. Schlegel, *J. Chem. Phys.*, 2004, **120**, 9918; (*c*) H. P. Hratchian and H. B. Schlegel, *J. Chem. Theory Comput.*, 2005, **1**, 61.

26 J. M. Goodman and M. A. Silva, *Tetrahedron Lett.*, 2003, **44**, 8233.

27 Y. Zhao and D. G. Truhlar, *J. Chem. Phys.*, 2006, **125**, 194101.

28 (*a*) F. Weigend and R. Ahlrichs, *Phys. Chem. Chem. Phys.*, 2005, **7**, 3297; (*b*) F. Weigend, *Phys. Chem. Chem. Phys.*, 2006, **8**, 1057.

29 G. Scalmani and M. J. Frisch, *J. Chem. Phys.*, 2010, **132**, 114110.

30 S. Grimme, J. Antony, S. Ehrlich and H. Krieg, *J. Chem. Phys.*, 2010, **132**, 154104.

31 M. J. Frisch, G. W. Trucks, H. B. Schlegel, G. E. Scuseria, M. A. Robb, J. R. Cheeseman, G. Scalmani, V. Barone, B. Mennucci, G. A. Petersson, H. Nakatsuji, M. Caricato, X. Li, H. P. Hratchian, A. F. Izmaylov, J. Bloino, G. Zheng, J. L. Sonnenberg, M. Hada, M. Ehara, K. Toyota, R. Fukuda, J. Hasegawa, M. Ishida, T. Nakajima, Y. Honda, O. Kitao, H. Nakai, T. Vreven, J. A. Montgomery Jr, J. E. Peralta, F. Ogliaro, M. Bearpark, J. J. Heyd, E. Brothers, K. N. Kudin, V. N. Staroverov, T. Keith, R. Kobayashi, J. Normand, K. Raghavachari, A. Rendell, J. C. Burant, S. S. Iyengar, J. Tomasi, M. Cossi, N. Rega, J. M. Millam, M. Klene, J. E. Knox, J. B. Cross, V. Bakken, C. Adamo, J. Jaramillo, R. Gomperts, R. E. Stratmann, O. Yazyev, A. J. Austin, R. Cammi, C. Pomelli,

J. W. Ochterski, R. L. Martin, K. Morokuma, V. G. Zakrzewski, G. A. Voth, P. Salvador, J. J. Dannenberg, S. Dapprich, A. D. Daniels, O. Farkas, J. B. Foresman, J. V. Ortiz, J. Cioslowski and D. J. Fox, *Gaussian 09, revision D.01*, Gaussian, Inc., Wallingford CT, 2013.

32 C. Y. Legault, *CYLview, 1.0b*, Université de Sherbrooke, Sherbrooke, Quebec, Canada, 2009, http://www.cylview.org.

33 (*a*) M. Ahlquist, P. Fristrup, D. Tanner and P.-O. Norrby, *Organometallics*, 2006, **25**, 2066; (*b*) M. Ahlquist and P.-O. Norrby, *Organometallics*, 2007, **26**, 550. for a related study, see also: (*c*) W.-J. Sun, W. Chu, L.-J. Yu and C.-F. Jiang, *Chin. J. Chem. Phys.*, 2010, **23**, 175. for a study on the speciation of $[Pd(Ph_3P)_4]$ in aromatic solvents, see: (*d*) P. Vidossich, G. Ujaque and A. Lledos, *Chem. Commun.*, 2014, **50**, 661.

34 Evaluation of this RMSD was performed by comparison of the single crystal X-ray structure from ref. 20 and the mirror image (*i.e.* the opposite enantiomer) of **7b-Cl**.

35 The structure of the IRC/QRC intermediates which follows the C–H bond activation step are presented in the ESI.† These structures are not included in the discussion herein due to the inaccuracy of DFT methods to describe salts that in the experimental conditions are present as solids and not as isolated molecules.

36 For a comprehensive review and reference therein, see: D. L. Davies, S. A. Macgregor and C. L. McMullin, *Chem. Rev.*, 2017, **117**, 8649.

37 J. I. Seeman, *Chem. Rev.*, 1983, **83**, 83.

38 For experimental and computational studies of the reactivity of unsymmetrical arynes in the absence of transition metals, see: (*a*) P. H.-Y. Cheong, R. S. Paton, S. M. Bronner, G.-Y. J. Im, N. K. Garg and K. N. Houk, *J. Am. Chem. Soc.*, 2010, **132**, 1267; (*b*) J. M. Medina, J. L. Mackey, N. K. Garg and K. H. Houk, *J. Am. Chem. Soc.*, 2014, **136**, 15798.

39 In the original publication, ethyl 3-phenylpropiolate was used experimentally.

40 Ligand exchange in the more stable intermediate **8** is possible but the resulting *trans* arrangement of the two carbon substituents would not allow direct C–C bond-forming reductive elimination. This would require an initial ligand dissociation and isomerization to form **28**.

41 The reactivity of this bond was confirmed by coupling compound 34 with *p*-tolylboronic acid under standard Suzuki-Miyaura reaction conditions utilizing $[Pd(Ph_3P)_4]$ as catalyst (see ESI†).